Targeted Delivery of Gemcitabine to Pancreatic Adenocarcinoma Using Cetuximab as a Targeting Agent

Chitta Ranjan Patra,[1] Resham Bhattacharya,[1] Enfeng Wang,[1] Aaron Katarya,[1] Julie S. Lau,[1] Shamit Dutta,[1] Michael Muders,[1] Shanfeng Wang,[2] Sarah A. Buhrow,[3] Stephanie L. Safgren,[3] Michael J. Yaszemski,[2] Joel M. Reid,[3] Matthew M. Ames,[3] Priyabrata Mukherjee,[1,4] and Debabrata Mukhopadhyay[1,4]

Departments of [1]Biochemistry and Molecular Biology, [2]Orthopedic Research, [3]Pharmacology and Experimental Therapeutics, and [4]Biomedical Engineering, Mayo Clinic, Rochester, Minnesota

Abstract

One of the key challenges in anticancer therapy is the toxicity and poor bioavailability of the anticancer drugs. Nanotechnology can play a pivotal role by delivering drugs in a targeted fashion to the malignant cells that will reduce the systemic toxicity of the anticancer drug. In this report, we show a stepwise development of a nanoparticle-based targeted delivery system for *in vitro* and *in vivo* therapeutic application in pancreatic cancer. In the first part of the study, we have shown the fabrication and characterization of the delivery system containing gold nanoparticle as a delivery vehicle, cetuximab as a targeting agent, and gemcitabine as an anticancer drug for *in vitro* application. Nanoconjugate was first characterized physico-chemically. *In vitro* targeting efficacy, tested against three pancreatic cancer cell lines (PANC-1, AsPC-1, and MIA Paca2) with variable epidermal growth factor receptor (EGFR) expression, showed that gold uptake correlated with EGFR expression. In the second part, we showed the *in vivo* therapeutic efficacy of the targeted delivery system. Administration of this targeted delivery system resulted in significant inhibition of pancreatic tumor cell proliferation *in vitro* and orthotopic pancreatic tumor growth *in vivo*. Tumor progression was monitored noninvasively by measuring bioluminescence of the implanted tumor cells. Pharmacokinetic experiments along with the quantitation of gold both *in vitro* and *in vivo* further confirmed that the inhibition of tumor growth was due to targeted delivery. This strategy could be used as a generalized approach for the treatment of a variety of cancers characterized by overexpression of EGFR. [Cancer Res 2008;68(6):1970–8]

Introduction

Adenocarcinoma of the exocrine pancreas is the fourth leading cause of cancer deaths in the United States (1).Currently, surgery is the only treatment, although due to its late presentation, only 9% to 15% of patients are suitable for surgery. The median survival for all stages of pancreatic cancer is ~3 to 5 months from diagnosis (2). Therefore, new therapeutic strategies are necessary to combat this deadly disease.

The underlying problem in the use of anticancer drugs is their toxicity and poor bioavailability (3). It is expected that if a nanoparticle-bearing anticancer drugs can be delivered in a targeted fashion, inhibition of tumor growth with reduced systemic toxicity will occur. We selected epidermal growth factor receptor (EGFR) as a target because pancreatic cancer cells overexpress EGFR (4, 5). It is also overexpressed in a variety of other cancers such as head and neck, renal, breast, colorectal, prostate, etc (6). We selected the anti-EGFR antibody Cetuximab (C225) as a targeting agent. C225 was approved by Food and Drug Administration (FDA) for the treatment of patients with EGFR-positive colorectal cancer (7–10). It is also approved for the treatment of non–small cell lung carcinoma, squamous cell carcinoma of the head and neck, and pancreatic cancer, underlining the importance of this strategy in other malignancies. Moreover, C225 was well-tolerated in early clinical studies; most frequent toxicity observed being the skin toxicity. It exhibited low immunogenicity as <4% of patient developed antichimeric antibodies in phase I clinical trials. We have selected gemcitabine as a cytotoxic agent as it is the current drug of choice for treatment of pancreatic cancer. In 1998, FDA approved gemcitabine for use in palliative treatment of patients with pancreatic carcinoma. It is found to have improvements in clinical benefit and survival compared with 5-fluorouracil (11). Moreover, gemcitabine is also used in the treatment of other malignancies such as head and neck, lung, breast, and ovarian cancers (12). Therefore, this strategy could be used as a generalized approach for the treatment of a variety of cancers including pancreatic cancer.

As a delivery vehicle, we selected gold nanoparticles (AuNP). The reasons for selecting AuNPs ~5 nm in size for this study are manifold: (*a*) recently, AuNPs have been used in various biomedical applications (13–25); (*b*) they are easy to synthesize and characterize due to the presence of a characteristic surface plasmon resonance (SPR) band and a low production cost (18, 26); (*c*) their surface chemistry is relatively simple and surface modification (attaching biomolecules) can be done fairly easily (27); and most importantly, (*d*) they are biocompatible and do not elicit toxic effects (17, 28, 29). Recent reports have shown the absence of chronic biochemical and hematologic toxicity in mice up to 1 year after injection of AuNPs (1.9 nm in diameter; ref. 28). Furthermore, the small size of these nanoparticles may allow them to escape uptake by mononuclear phagocytic cells and penetrate through the smallest capillary pores within the human vasculature (17, 30).

We successfully fabricated and characterized AuNPs with C225 and gemcitabine on a single gold core (Au-C225-Gem). We have

Note: Supplementary data for this article are available at Cancer Research Online (http://cancerres.aacrjournals.org/).

C. R. Patra and R. Bhattacharya contributed equally.

Current address for S. Wang: Department of Materials Science and Engineering, The University of Tennessee, Knoxville, TN 37996.

Requests for reprints: Priyabrata Mukherjee, Department of Biochemistry and Molecular Biology, Department of Biomedical Engineering, Mayo Clinic, Rochester, MN 55905. Phone: 507-284-8563; Fax: 507-284-1767; E-mail: mukherjee.priyabrata@mayo.edu.

doi:10.1158/0008-5472.CAN-07-6102

also shown that Au-C225-Gem is far more effective in inhibiting tumor cell proliferation *in vitro* and tumor growth *in vivo* compared with its nontargeted counterpart. Pharmacokinetic experiments along with quantitation of gold in targeted versus nontargeted delivery both *in vitro* and *in vivo* further confirmed that the inhibition of tumor growth was due to targeted delivery. This is the first report that describes that targeted delivery of a cytotoxic drug as a gold nanoconjugate can efficiently inhibit *in vivo* tumor growth in orthotopic tumor model of pancreatic cancer.

Materials and Methods

Reagents. Tetrachloroauric acid ($HAuCl_4$) and sodium borohydride ($NaBH_4$) were purchased from Aldrich Chemicals. Gemcitabine was purchased from Eli Lily. C225 was purchased from Bristol-Myers Squib. The anti-EGFR antibody for Western blot analysis was purchased from Santa Cruz Biotechnology (sc-03).

Cell culture. The pancreatic cancer cell lines AsPC-1, PANC-1, and MIA Paca-2 was purchased from American Type Culture Collection and cultured using RPMI 1640 (Cellgro Mediatech, Inc.) with L-glutamine and 1% penicillin-streptomycin (Invitrogen).

Synthesis of AuNPs. AuNPs were synthesized from $HAuCl_4$ using NaBH4 as a reducing agent as previously described (Supplementary Data; ref. 31).

Synthesis of gold nanoconjugates containing anti-EGFR antibody or gemcitabine. The synthesis of gold-EGFR antibody conjugates was performed by incubating anti-EGFR antibody with a nanoparticle suspension at pH 7.8. The saturation concentration of anti-EGFR was determined by incubating different concentrations of the antibody with the AuNPs followed by stability testing using a 140 mmol/L sodium chloride (NaCl) solution. Eight tubes, each containing 1 mL of AuNPs, were incubated with increasing concentrations of C225 (anti-EGFR) for 1 h, followed by treatment with a NaCl solution to a final concentration of 140 mmol/L. Fifteen minutes after the incubation with NaCl, the UV-visible spectra were recorded on a Shimadzu spectrophotometer (UV2401 PC), and the saturation concentration was determined. Similarly, the saturation concentration of gemcitabine on AuNPs was determined.

Fabrication of a gold nanoconjugate containing C225 and gemcitabine on a single gold core. To attach both gemcitabine and C225 to AuNP, incubation experiments were carried out below the 50% saturation concentration of both reagents. AuNPs were first incubated for 1 h at room temperature with 2 μg/mL of C225 at pH 7.8 followed by another 1 h incubation with 5 μg/mL of gemcitabine. For aggregation experiments, 140 mmol/L NaCl solution was added to the above solution and incubated for another 15 min. Subsequently, UV-visible spectra were recorded. For our *in vitro* and *in vivo* studies, a large batch was prepared by incubating 300 mL of AuNPs with 600 μg of C225 and 1.5 mg of gemcitabine as described above. After the final incubation, the nanoconjugates were concentrated by ultracentrifugation (Sorvall Ultracentrifuge OTD80B using 50.2 Ti Rotor) at 20,000 rpm for 45 min at 10°C. The purified nanoconjugates were UV irradiated for 15 to 20 min before *in vitro* and *in vivo* studies.

Thermogravimetric analysis. For performing thermogravimetric analysis (TGA) of Au-C225, 150 mL AuNPs were incubated with 300 μg of C225. After 1 h, the nanoconjugates were centrifuged at 20,000 rpm for 45 min, freeze dried overnight, and analyzed using TGA. Similarly, for TGA analysis of Au-C225-Gem, 150 mL AuNPs were incubated with 300 μg of C225 (2 μg/mL). After 1 h, the nanoconjugates were further incubated for 1 h with 750 μg of gemcitabine (5 μg/mL), centrifuged at 20,000 rpm for 1 h, freeze dried overnight, and analyzed using TGA. The quantification and attachment of gemcitabine was further confirmed by high performance liquid chromatography (HPLC) of the resulting supernatant after ultracentrifugation.

X-ray photoelectron spectroscopy. X-ray photoelectron spectroscopy (XPS) was performed on a PHI 5400 instrument using a Mg Kα X-ray (1,253.6 eV) anode source operated at 250 W under a pressure below 2×10^{-9} torr, as described previously. Samples were prepared by drop coating the gold nanoconjugate solution on a clean silicon wafer, and the drops were allowed to air dry before the measurement (Supplementary Data; ref. 32).

***In vitro* release studies of gemcitabine from "2 in 1" conjugates.** The quantification of gemcitabine and C225 in the nanoconjugate was already described in the experimental section. The loose pellet obtained after ultracentrifugation (as described above) was divided into several fractions. Each fraction was diluted with equal amount of PBS and incubated at 37°C for a defined period of time. After the incubation, the solutions were ultracentrifuged at 40,000 rpm at 10°C for 1 h in a Beckman TL-100 ultracentrifuge using a TLA-100.2 rotor, and the amount of gemcitabine released into the supernatant was measured by HPLC.

Western blot analysis. The expression of EGFR protein was determined in untreated AsPC-1, PANC-1, and MIA Paca2 cells by Western blot analysis (Supplementary Data).

***In vitro* targeting of Au-C225 to cancer cells expressing EGFR receptor.** Confluent AsPC-1, PANC-1, and MiA Paca-2 cells in 100-mm tissue culture dishes (in triplicate) were treated for 2 h with the purified conjugates obtained after ultracentrifugation. The 2-h treatment was chosen based on previous reports on the internalization of AuNPs, which stated that longer time points did not increase gold uptake nor did it alter the pattern of internalization (33). After the 2-h treatment, cells were thoroughly washed thrice with PBS, trypsinized, and washed again in PBS. Cells were pooled together from three plates and finally spun down at 1,300 rpm to obtain the pooled pallet to get the optical picture and then either fixed in Trumps solution for transmission electron microscopy (TEM) sectioning and imaging under a TEM microscope or resuspended in PBS for inductively coupled plasma (ICP) analysis. Humanized IgG was used as an isotype control for C225, and the cells were treated with Au-IgG similarly as described above.

***In vitro* cell proliferation assay.** AsPC-1 cells (2×10^4) were seeded in 24-well plates, cultured for 1 d in RPMI 1640 supplemented with 10% fetal bovine serum, 5% L-Glutamine, and 1% antibiotics. Cells were then incubated with different doses of gemcitabine either in the form of a "2 in 1" nanoconjugate (as Au-Anti–EGFR-Gem) or as free gemcitabine in an equimolar mixture of C225 and gemcitabine (C225 + Gem). After 2 h of incubation, cells were washed thrice with PBS and finally resuspended with RPMI 1640 containing serum and antibiotics. After culture for 72 h, 1 μCi [^{3}H]-thymidine was added and proliferation assay was performed as previously described (32). Experiments were repeated at least thrice and in triplicate.

Generation of orthotopic model of pancreatic cancer, noninvasive imaging, and treatment schedule. AsPC-1 cells were infected with a lentiviral reporter gene construct containing the bioluminescent reporter genes firefly luciferase and green fluorescent protein (GFP). Cells were sorted using fluorescence-activated cell sorting to obtain a pure population of cells expressing GFP/luciferase. The isolated cells (2×10^6) were then orthotopically injected into the pancreas of nude mice (ages 4 to 6 wk) as described previously (34). On day 4 postinjection, bioluminescence was measured and the mice were randomized into several groups before the initiation of treatment. *In vivo* optical imaging for luciferase was done ~20 min after i.p. injection of 3 mg n-Luciferin into each animal using a Xenogen-IVIS–cooled CCD optical system (Xenogen-IVIS). The doses were 4 mg/kg/dose of C225, either bound (as in Au-C225-Gem) or free, and 2 mg/kg/dose gemcitabine, either bound (as in Au-anti–EGFR-Gem) or free. As controls, we used an equimolar mixture of C225 and gemcitabine (C225 + Gem), Au-C225 (containing 4 mg/kg of C225), or Au-IgG (4 mg/kg of IgG). The injection schedule was thrice the 1st wk followed by twice on wk 2 and 3. All mice were sacrificed the day after the last injection but before a final bioluminescence measurement.

Biodistribution of gold using ICP. After the generation of orthotopic pancreatic tumor models, we injected the nude mice i.p. with Au-C225, Au-IgG, and Au-C225-gemcitabine and as (C225 + Gem) in separate groups as described in the treatment schedule (4 mg C225/kg/dose in a gold-bound form, i.e., Au-C225 or Au-C225-gem or 4 mg IgG/kg/dose for the isotype control Au-IgG). The treatment schedule was thrice in the 1st wk followed by twice for subsequent weeks. The day after the last injection, all mice were sacrificed and different organs (mainly liver and kidney) were collected for gold analysis. The gold uptake in different organs was measured using ICP analysis (Supplementary Data).

Pharmacokinetics. Pharmacokinetics of gemcitabine and gold in the nanoconjugates were characterized in 4- to 6-wk-old nude mice (three mice per time point). The mice were injected i.v. through the tail vein with 2 mg/kg of gemcitabine alone or Gem-Au-C225 (2 mg/kg was used to test the therapeutic efficacy). Blood samples were collected from the mice under isoflurane anesthesia 2, 5, 15, 30, 60, and 120 min after drug administration in heparinized tubes containing tetrahydrouridine to prevent gemcitabine degradation by cytidine deaminase. Gemcitabine and its major plasma metabolite dFdU were determined using normal phase HPLC according to the published literature procedure (35). The amount of gold present in serum was quantified using ICP as described in the Supplementary Data.

TEM of cells treated with nanoconjugates. TEM sample preparation involving cells were performed as previously described (33). After the incubation with nanoconjugates, cells were trypsinized and centrifuged initially at 1,500 rpm for 5 min (Supplementary Data).

Results and Discussion

Synthesis of AuNPs. Physicochemical characterizations of AuNPs formed by the $NaBH_4$ method were performed using TEM and UV-visible Spectroscopy. As previously reported (31), the UV-Visible spectrum of AuNPs exhibited characteristic SPR bands at ~512 nm, suggesting the formation of spherical AuNPs. The ~5 nm size of the nanoparticles was further confirmed by TEM (data not shown).

Saturation concentration of C225 and gemcitabine and stability of the nanoconjugates. A rough approximation of the amount of any protein or drug needed for saturating AuNPs can be obtained from their respective saturation curve. Aggregation of uncovered or partially covered particles is induced by the addition of 140 mmol/L NaCl and can be monitored by following the SPR absorbance of AuNPs. The concentration minimizing aggregation is considered to be the saturation concentration. The extent of aggregation, however, should decrease with increasing protection of the AuNP surface either by antibody or by gemcitabine. It is clear from Fig. 1*A* that in the absence of any antibody but in the presence of NaCl, AuNPs completely aggregated and their absorbance dropped to zero. Protecting the AuNP surface with C225 prevented aggregation. The extent of aggregation was found to be minimal at a C225 concentration of 4 μg/mL. The absorbance also reached a maximum at 4 μg C225/mL of AuNP solution. The shift in the λ_{max} value of the above samples (Fig. 1*B*) exhibited a similar trend where the shift reached a maximum in the absence of any stabilizing antibody and minimum with a C225 concentration of 4 μg/mL. The shift in the λ_{max} values and change in the absorbance of the AuNP solution with a gradual increase in antibody concentration suggest that the saturation concentration of C225 on AuNP is 4 μg/mL. The observed red shift in the λ_{max} value and an increase in plasmon resonance are consistent with a increase in the dielectric constant of the medium surrounding the AuNPs and suggest the conjugation of C225 to AuNP (36). The saturation concentration of gemcitabine on AuNPs was also determined separately as described above and it is found to be 20 μg/mL (data not shown).

Fabrication of "2 in 1" nanoconjugates containing both C225 and gemcitabine on a single gold core. Incubation experiments were performed to synthesize Au-C225-Gem at a 50% saturation concentration of C225 and a 25% saturation concentration of gemcitabine. The SPR absorption gradually increased with the addition of C225 and gemcitabine, indicating a better stabilization of AuNPs bound to both components rather than to an individual component, as expected (Fig. 1*C*). A similar trend was also observed in a shift of λ_{max} values and an aggregation test with NaCl solution, confirming that the nanoconjugates containing both C225 and gemcitabine (Gem-Au-C225) on a single gold core are more stable than gold conjugates containing a single agent (Au-C225 or Au-Gem; data not shown).

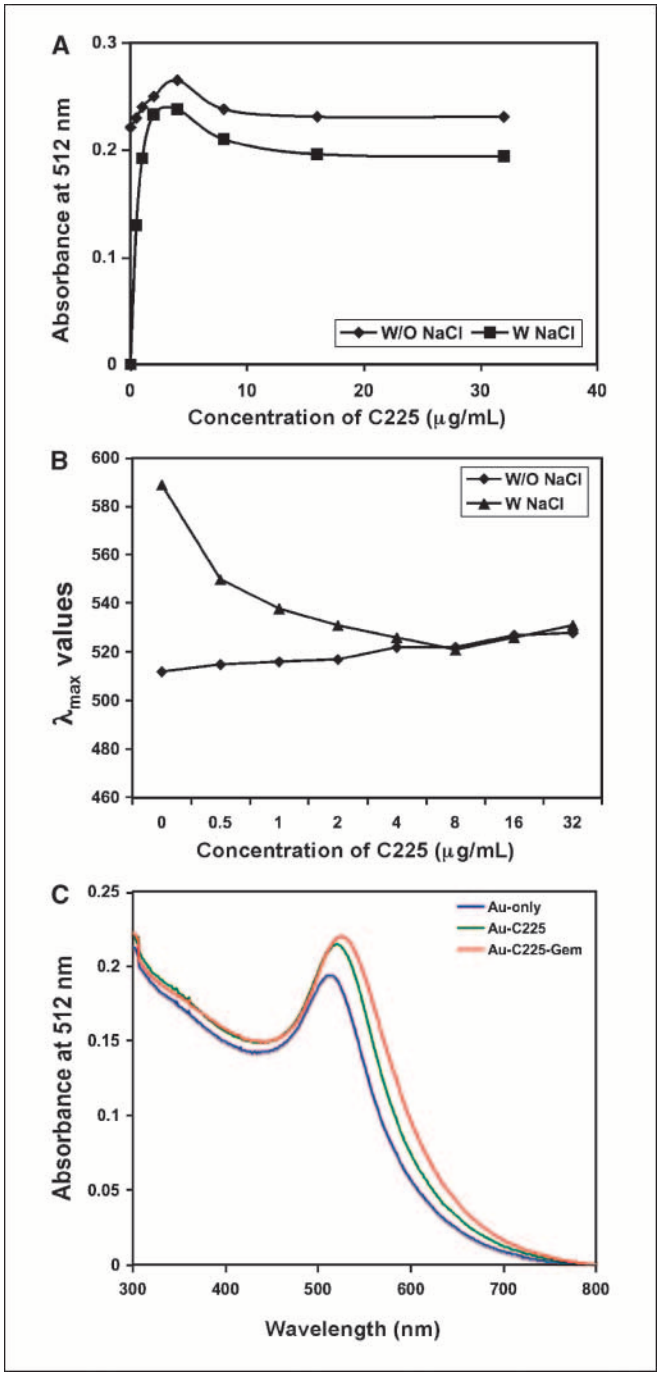

Figure 1. The synthesis of gold-EGFR antibody conjugates was performed by incubating anti-EGFR antibody with a nanoparticles suspension at pH 7.8. The saturation concentration of anti-EGFR was first determined by incubating different concentrations of the antibody with the AuNPs followed by stability testing using a 140 mmol/L NaCl solution. *A* and *B*, determination of saturation curve of C225 on AuNPs with or without the presence of NaCl, change in absorbance of AuNP, and shift in the λ_{max} with the addition of increasing concentration of C225. *C*, change in absorbance of AuNPs with the addition of C225 and gemcitabine.

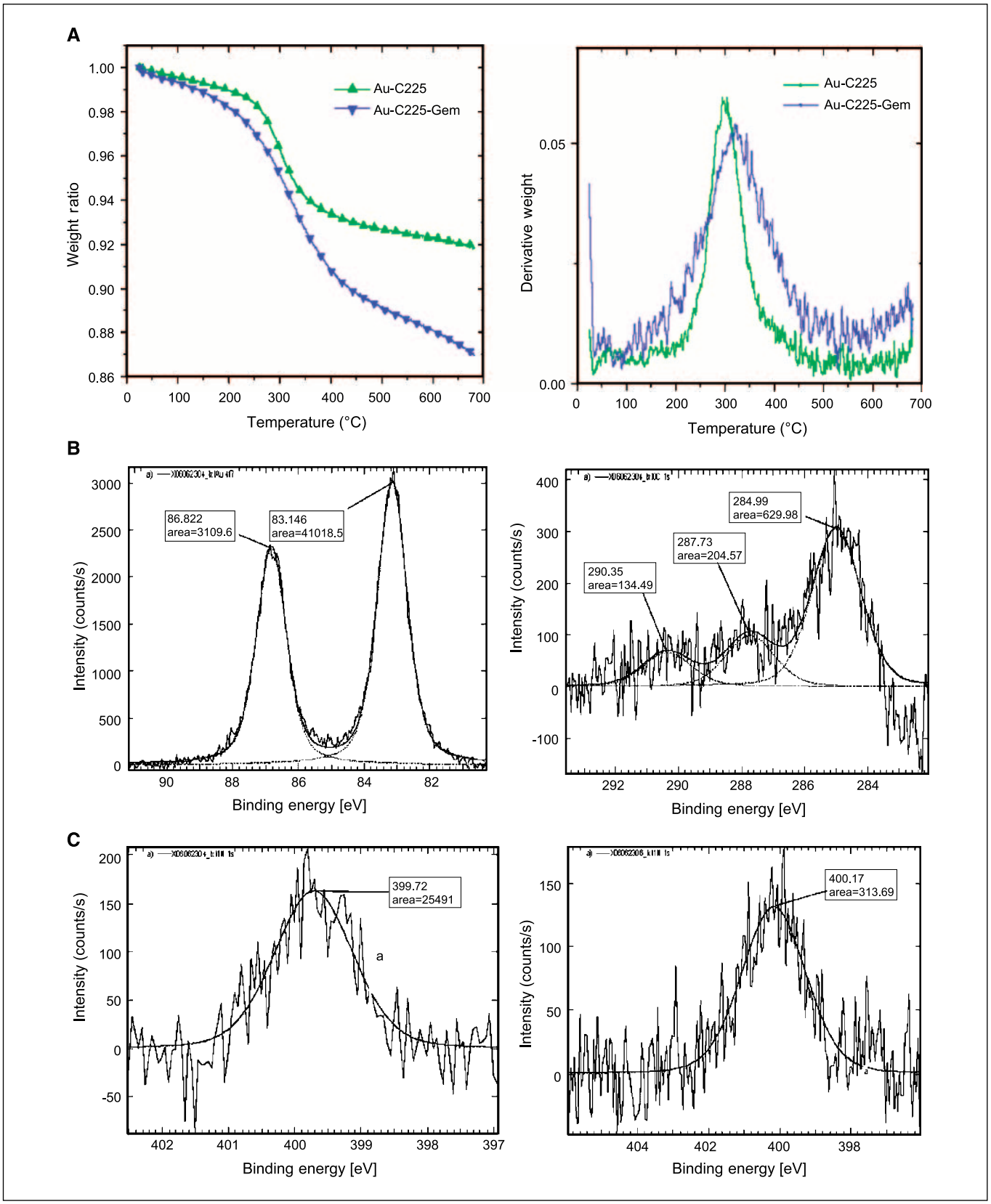

Figure 2. Quantitation of gemcitabine and C225 bound to AuNPs and their nature of bonding is shown by TGA and XPS Lyophilized powder of purified nanoconjugates used for these studies (see Materials and Methods). *A,* weight loss of the conjugate over temperature (*left*) and derivative of weight loss over temperature (*right*). *B,* XPS spectra (core level binding energy) of gold (*left*) and carbon from Au-C225 conjugates (*right*). *C,* core level binding energy of N obtained from Au-C225 (*left*) and Au-C225-Gem (*right*), respectively.

It is already reported that antibody has the ability to bind covalently to AuNP due to the presence of thiols/amine groups present within the amino acid residues (16, 37). Therefore, we speculate that C225 also uses similar bonding mode with AuNP. Quantitation of the amount of C225 and gemcitabine bound to AuNP and their nature of bonding was further confirmed by TGA and X-ray photoelectron spectroscopy (XPS) as discussed below.

Quantitation of C225 and gemcitabine in Au-C225-Gem nanoconjugates. Figure 2*A* represents the TGA profile (*left*) and derivative weight ratio (*right*) of Au-C225 and Au-C225-gem nanoconjugates, respectively. Theoretically, the weight loss for C225 should be 7% and 15% for gemcitabine (where 1 mL AuNP solution containing 26 μg of gold was incubated with 2 μg of C225 and 5 μg of gemcitabine). It is clear that a weight loss of 5% was observed in the Au-C225 sample, whereas a weight loss of 8% was observed for the Au-C225-Gem sample. In both cases, the maximum desorption/decomposition took place at ~300°C (Fig. 2*A*). Therefore, the weight loss for gemcitabine in Au-C225-gem was 3%. Hence, the TGA data confirmed that of the C225 and gemcitabine initially used for the incubation, 71% of C225 and 20% of gemcitabine, were attached to the AuNPs as Au-C225-Gem. Similar conjugations were also observed in the case of Au-IgG-Gem (isotype control of Au-C225-Gem). According to previous reports, the resultant weight loss at ~300°C is typical of Au-SH and Au-NH_2 covalent bonding energy (16, 33). However, in the case of Au-C225-Gem, the desorption/decomposition maxima shifted to ~320°C, suggesting additional stabilization of the nanoconjugates that needed a higher energy to desorb/decompose the antibodies/drugs from the AuNP surface. The result obtained from TGA was further confirmed by HPLC of the supernatant solution after ultracentrifugation, revealing 80% of the gemcitabine initially used to bind to AuNP was found in the supernatant.

Nature of bonding between C225 and gemcitabine with AuNP: XPS analysis. The covalent bonding as suggested by the TGA analysis was further confirmed by XPS shown in Fig. 2*B* to *C*. Figure 2*B* (*left*) exhibits a single gold (Au 4f7/2) peak at 83.1 eV with a spin orbit coupling of 3.7 eV in the drop-coated conjugates. These data show that the Au^{+3} ions used in this process were reduced to Au^0 by $NaBH_4$ (16, 17). Figure 2*B* (*right*) shows the presence of three carbon peaks at 284.9, 287.3, and 290.3, and they are sp^3- (in saturated hydrocarbons such as in diamond) and sp^2-hybridized carbons (such as in C = C and C = O). Two weak sulfur peaks were also observed. The presence of two sulfur peaks at ~162 and 166 eV represented two chemically distinct sulfur species. However, the peaks were too weak to be curve fitted (data not shown). We observed similar sulfur peaks from gold conjugates containing the VEGF165 growth factor (32) as well gold conjugates containing the monoclonal antibody to VEGF165 (anti-VEGF165; ref. 16). According to previous reports, the peak at ~162 eV can be assigned to a gold-thiolate bond and peaks at a higher binding energy to sulfones (16, 38). The nitrogen 1s peak at 399.6 eV (Fig. 2*C, left*) is likely due to unionized, nonprotonated nitrogen (32). This is in agreement with earlier studies reporting adsorption of proteins/amino acids or amines on gold surfaces (39). It is also

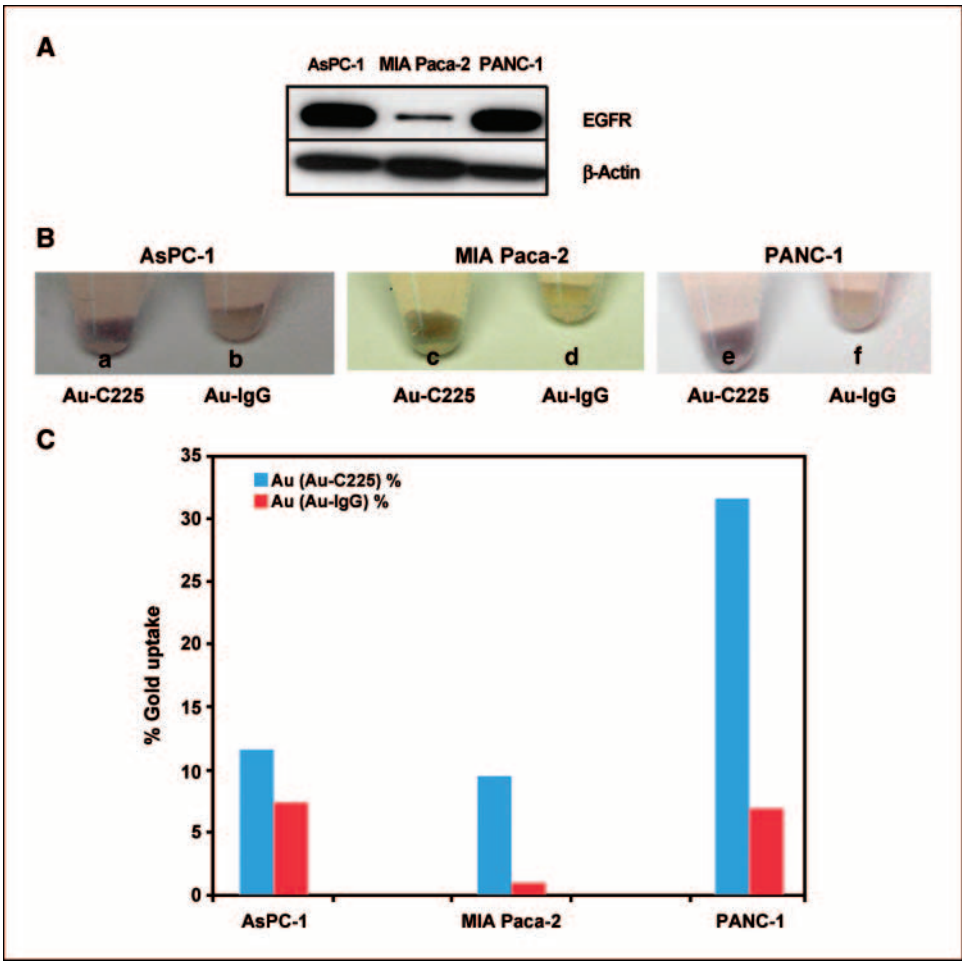

Figure 3. *In vitro* targeting of EGFR-expressing cells using Au-C225. Confluent AsPC-1, PANC-1, and MIA Paca-2 cells in 100-mm tissue culture dishes (in triplicate) were treated for 2 h with the purified conjugates obtained after ultracentrifugation and processed for optical micrography, TEM, ICP analysis, and Western blot measurements. *A,* EGFR expression pattern in different cells via Western blot. *B,* optical picture of different cells treated with Au-C225 and Au-IgG. *C,* quantitative estimation of gold uptake by different cells using ICP.

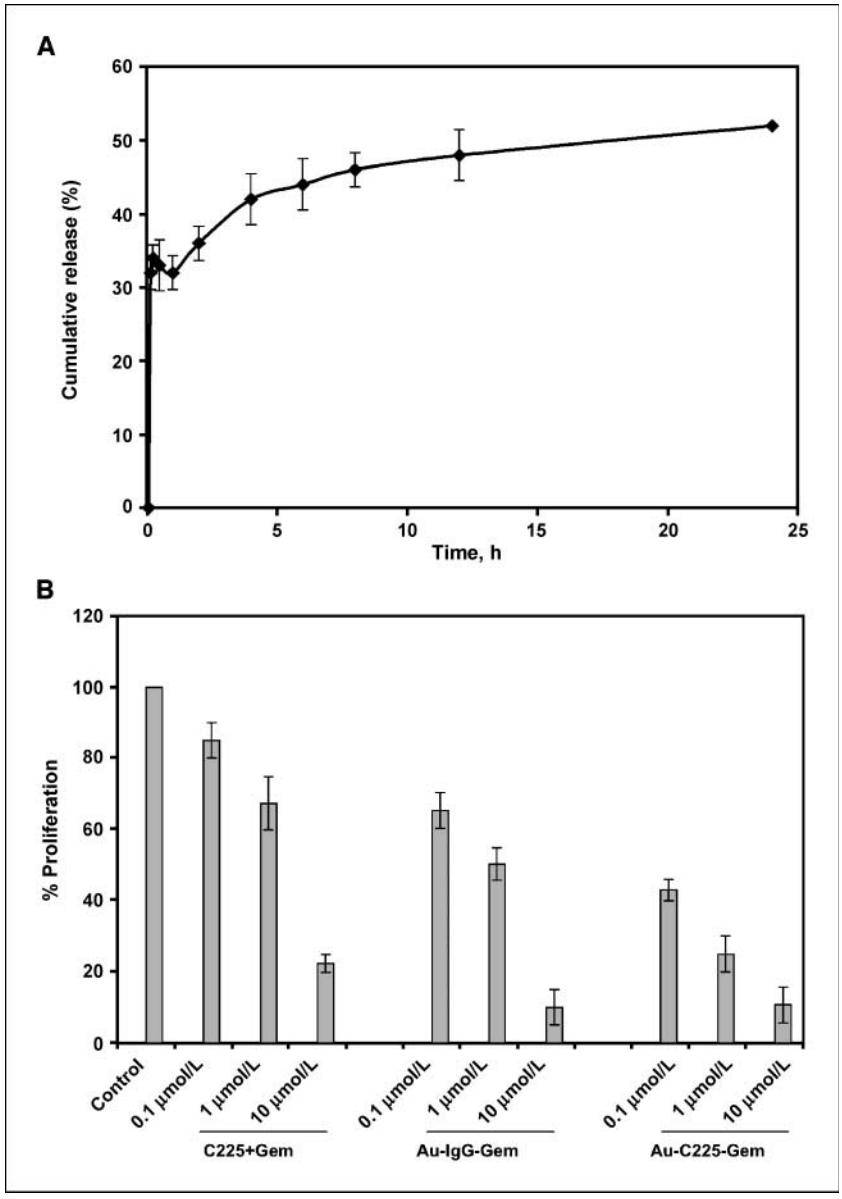

Figure 4. Release profile of gemcitabine from the purified nanoconjugates in phosphate buffer saline and *in vitro* efficacy of the nanoconjugate to inhibit AsPC-1 cell proliferation *in vitro*. The loose pellet obtained after ultracentrifugation was divided into several fractions. Each fraction was diluted with an equal amount of PBS, incubated at 37°C for a defined period of time, and spun down by ultracentrifugation. The amount of gemcitabine released into the supernatant was measured by HPLC. *A, in vitro* release profile of gemcitabine over time in PBS. *B,* comparative study of the *in vitro* efficacy of Au-C225-gem with its isotype control Au-IgG-Gem and a equimolar combination of C225 and gemcitabine (C225 + Gem) to inhibit proliferation of AsPC-1 cells as determined by ^{3}H incorporation assay.

interesting to note that the contribution from the nitrogen 1s peak observed in Au-C225-Gem is higher than that of Au-C225, suggesting that this contribution may be from the gemcitabine nitrogen (Fig. 2*C, right*). Furthermore, the nitrogen peak in Au-C225-Gem was shifted to a slightly higher energy, suggesting a covalent bonding of the gemcitabine nitrogen to AuNPs that shifted the N 1s core level peak to a higher binding energy (similar observations were made from TGA as well).

Gemcitabine is a pyrimidine nucleoside and, hence, a weak nucleophile. Therefore, the bonding between gemcitabine and AuNPs are expected to be weaker. However, the TGA data and XPS studies show that gemcitabine binds to AuNPs fairly strongly (desorption temperature, ~320°C), suggestive of a covalent bond. Stability studies in 140 mmol/L NaCl also suggest a similar mode of bonding. Furthermore, the nature of bonding between DNA bases and nucleosides on gold are well-reported in the literature (40). Recently, it has been described that the ($C-NH_2$) part of the adenine molecule changes configuration from planar (sp^2) to nonplanar (sp^3) upon coordination to metals, suggesting a covalent bonding between DNA bases and nucleosides on gold (40). In brief, stability experiments, TGA, and XPS analysis as well as reports in the literature suggest the covalent nature of bonding between gold and C225 and between gold and gemcitabine.

***In vitro* targeting of Au-C225 to pancreatic cancer cells with variable EGFR expression.** Before testing the nanoconjugate for the functional activity of individual component, it is important to determine the targeting efficacy of the nanoconjugate. To validate the efficacy of C225 as a targeting agent and viability of EGFR as a target, we determined the EGFR expression levels in three different pancreatic cancer cell lines, namely AsPC-1, PANC-1, and MIA Paca2 by Western blot analysis. If EGFR is a viable target, it is expected that cells with highest EGFR levels will uptake maximum amount of Au-C225 compared with the one with lower expression. The uptake of Au-C225 can be quantified in terms of gold using ICP. The Western blot analysis clearly shows that AsPC-1 and PANC-1 express higher levels of EGFR than MIA Paca2 cells (Fig. 3*A*). To check the viability of EGFR as a target, all the cells were treated with the purified conjugates for 2 hours (described in

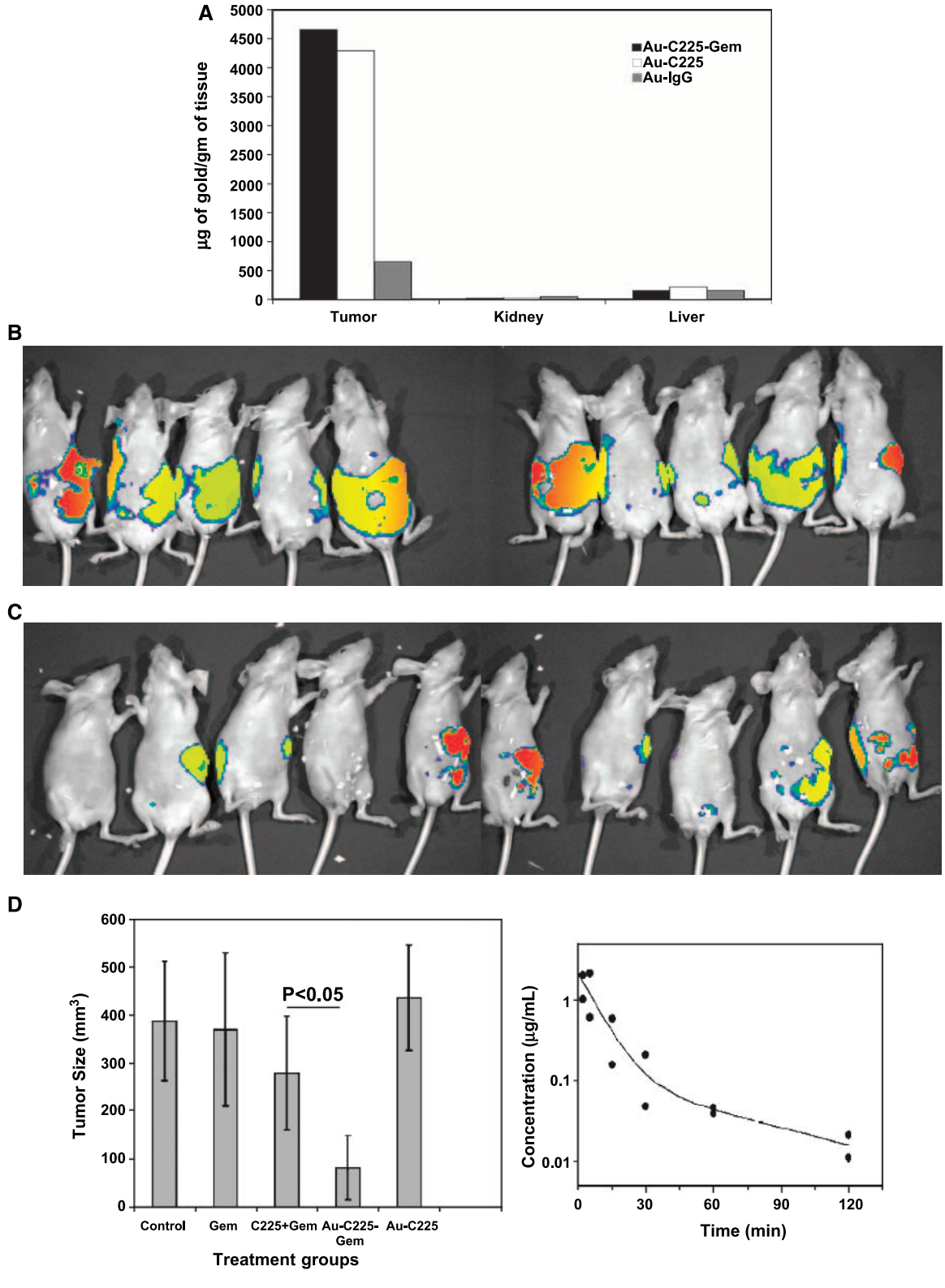

Figure 5. *In vivo* targeting of the nanoconjugate and its therapeutic efficacy. *A,* the quantification of the amount of gold taken up by the tumor, kidney, and liver under different treatment groups ($n = 3$). A comparative bioluminescence image from the mice treated with a mixture of C225 and gemcitabine (C225 + Gem; *B*) or Au-C225-Gem (*C*) i.p. ($n = 10$). *D,* effect of different treatment groups on tumor growth inhibition *in vivo* (*left*). Tumor volume was measured after sacrificing the mice at the end of the experiment. *Right,* plasma concentration of gold over time determined by ICP analysis. Blood samples were collected from the mice under isoflurane anesthesia at different time points in heparinized tubes containing tetrahydrouridine to prevent gemcitabine degradation by cytidine deaminase after i.v. drug administration.

Materials and Methods). An optical picture of all the different cells after treatment with Au-C225 and its isotype control Au-IgG is shown in the Fig. 3*B*. The figure shows that all the cells efficiently uptake Au-C225 as evidenced by the deep blue color of the cell-pellet, whereas Au-IgG was minimally taken up. Uptake was further quantified by ICP analysis. ICP analysis showed that cells with higher EGFR expression internalized maximum Au-C225, whereas cells with lowest expression had minimal uptake (Fig. 3*C*), demonstrating that EGFR could be an efficient target, at least *in vitro*, for cell specific delivery of nanoparticles or drug/antibodies. This is further supported by TEM analysis (Supplementary Fig. S1). It is also interesting to note here that PANC-1 and MIA Paca-2 showed better specificity of targeting compared with AsPC-1, although it has high EGFR expression. This may be due to the fact that both PANC-1 and MIA Paca-2 are primary cell lines, whereas AsPC-1 is a metastatic cell line. Therefore, to test the efficacy of the targeted delivery system in a metastatic model, we used AsPC-1 in our *in vivo* studies as it generates the most aggressive form of tumor when implanted orthotopically that mimics the human situation. To further confirm the internalization of Au-C225 and its location, we performed TEM analysis of Au-C225– and Au-IgG–treated AsPC-1 cells, respectively. Efficient internalization of Au-C225 was seen in TEM, whereas Au-IgG was only marginally taken up by the cells (Supplementary Fig. 1). We found similar cellular uptake of Au-C225-Gem by these cells. Therefore, all of the experiments discussed above clearly suggest that gold nanoconjugates containing C225 could be an efficient vehicle to deliver anticancer drugs to a pancreatic tumor in a targeted fashion.

***In vitro* release profile of gemcitabine from Au-C225-Gem.** To successfully deliver the nanoconjugate *in vivo*, the nanoconjugate needs to be stable enough to reach the desired target before any dissociation. Therefore, it is extremely important to study the release profile of gemcitabine from Au-C225-Gem under physiologic conditions. The release profile of gemcitabine in the conjugate was tested in normal PBS at a physiologic pH of 7.4. The Au-C225-Gem was obtained by ultracentrifugation and divided into several equal fractions. Each fraction was diluted with equal amount of PBS and incubated at 37°C for a defined time period (described in Materials and Methods) followed by ultracentrifugation. The amount of gemcitabine released over time into the supernatant was measured by HPLC. Figure 4*A* describes the *in vitro* release profiles of gemcitabine from Au-C225-Gem nanoconjugate, demonstrating that only 30% to 40% of AuNP-bound gemcitabine was released after a 6-hour incubation period, and ~45% was released from the nanocomposite over a period of 24 hours. These results suggest sufficient stability of the nanoconjugates in a physiologic salt concentration.

***In vitro* functional efficacy of Au-C225-Gem.** Before *in vivo* studies are performed, it is important to show the functional activity of gemcitabine in Au-C225-Gem and whether the *in vitro* targeted delivery of gemcitabine results in enhanced inhibition of tumor cell proliferation. In Fig. 4*B*, significant inhibition of AsPC-1 proliferation was observed with Au-C225-Gem compared with its nontargeted counterpart, Au-IgG-Gem or single-agent alone (Gem only or C225 only), or an equimolar mixture of the agents (Gem + C225). A dose-dependent inhibition of proliferation was observed in all the groups with maximum inhibition with Au-C225-gemcitabine. Au-IgG-Gem also inhibited significantly when compared with an equimolar mixture of C225 and gemcitabine, suggesting that conjugation to AuNP increases the efficacy of gemcitabine when tested in a closed cell culture system. It is also important to note that neither Au-C225 nor Au-IgG had any effect on the proliferation of AsPC-1 cells (data not shown).

EGFR-mediated targeting of gold nanoconjugates *in vivo*. After elucidating the *in vitro* efficacy of the nanoconjugates, we wanted to determine whether C225 could efficiently deliver Au-C225-Gem to the tumor *in vivo*. To test the efficacy of the targeted delivery system in a metastatic model, we used AsPC-1 in our *in vivo* studies as it generates the most aggressive form of tumor when implanted orthotopically that mimics the human situation. Generation of the orthotopic tumor model of pancreatic cancer using AsPC-1 cells and treatment schedule is described in Materials and Methods. Biodistribution of gold in different tissues was performed using ICP, and results were shown in Fig. 5*A*. C225 could efficiently home Au-C225-Gem to the tumor as evidenced by the gold content detected among the various treatment groups. Furthermore, the presence of gemcitabine did not interfere with the targeting ability of C225 as there was no significant difference in the gold content of tumors in the Au-C225 group and Au-C225-Gem group. The gold uptake in the kidney and liver was also minimal. These data conclusively prove that efficient *in vivo* delivery of gold nanoconjugates to a pancreatic tumor could be achieved by using the anti-EGFR antibody as a targeting agent.

Therapeutic efficacy of the nanoconjugates *in vivo*. After demonstrating the ability of C225 to target EGFR-expressing cells both *in vitro* and *in vivo*, we wanted to investigate if the same nanoconjugates could inhibit tumor growth *in vivo*. After orthotopically implanting AsPC-1/luciferase tumor cells in the pancreas, mice were noninvasively imaged for luciferase bioluminescence using the Xenogen instrument (described in Materials and Methods) to check for tumor growth and randomized thereafter before the initiation of the treatment. Figure 5*B* and *C* represented the luciferase imaging of the control group (C225 + Gem) and experimental group (Au-C225-Gem), respectively, at the end of the study. These figures clearly show significant tumor growth inhibition in mice treated with Au-C225-Gem compared with its nontargeted counterpart. These results were further confirmed by measuring the tumor growth after sacrificing the mice at the end of the experiment and assessing the tumor volumes. Figure 5*D* (*left*) clearly shows that Au-C225-Gem inhibited tumor growth significantly (~80%) compared with all other nontargeted groups.

It was previously reported that in orthotopic pancreatic tumor model, a dose of 250 mg/kg of gemcitabine resulted in a 58% inhibition of tumor growth, and a dose of 7.5 mg/kg did not inhibit tumor growth significantly (41). It is important to stress that we used a much lower dose (2 mg/kg) of the drug than previously used in preclinical studies. We reasoned that if the drug was successfully delivered in a targeted fashion, we should see growth inhibition at a lower dose, and this was shown in our experiment. Furthermore, the absence of any inhibition in the gemcitabine only group is probably due to this low dose. It is also important to note that neither the combination group (C225 + Gem) nor the Au-C225 group inhibited tumor growth significantly, possibly due to the low dose of the drug. We also did not see significant effect with Au-IgG-Gem group probably due to lack of targeting of the nanoconjugate (data not shown).

Pharmacokinetics of Au-C225-Gem. Inhibition of tumor growth with such a low dose of gemcitabine is very significant and will have strong implications in cancer treatment where toxicity is a major concern. To test whether the efficacy observed at

a lower dose is due to increased retention of gemcitabine in the circulation upon nanoconjugation, we checked the clearance of Au-C225-Gem from circulation in terms of gold concentration with pharmacokinetic experiments. If gemcitabine were retained in the circulation as gold nanoconjugates, we would expect enhanced retention of gold in the circulation. Mean gold concentration data were fit to a two-compartment open model using the program Winnonlin, version 4.1 (Pharsight Corp.) weighted by the inverse of the concentration squared. Biexponential decline in the gold plasma concentration was observed with an initial distribution half-life of 5.63 minute and a terminal elimination half-life of 41.8 minute (Fig. 5*D, right*). We also did not observe any increased gemcitabine retention upon nanoconjugation when compared with free gemcitabine (data not shown). These findings prove that the efficacy observed at a lower dose is due to targeted delivery and not due to increased retention upon nanoconjugation.

Targeted delivery of anticancer drugs specifically to the tumor site is an important area of research in cancer therapeutics. Tumor-specific delivery of anticancer drugs will maximize the efficacy of the drug and minimize collateral damage and, hence, reduce systemic toxicity. In this article, we have shown the fabrication of gold nanoconjugates containing a targeting agent and a cytotoxic drug. It is important to note that targeted delivery is not only dependent on EGFR expression but also on the mechanism of receptor endocytosis and dynamics. A clear correlation of EGFR expression with gold uptake is observed in primary pancreatic cancer cell lines (high in PANC-1 and low in MIA Paca-2), whereas gold uptake is low in metastatic AsPC-1 cell line, although it expresses similar levels of EGFR as PANC-1. More importantly, we have shown that the nanoconjugates containing gemcitabine and C225 can specifically reach the metastatic tumor cells both *in vitro* and *in vivo* with enhanced efficacy. Future technological advantages associated with AuNPs may be used in cancer therapeutics.

Acknowledgments

Received 11/5/2007; revised 1/11/2008; accepted 1/16/2008.

Grant support: Chronic Lymphomic Leukemia-Global Foundation grant (CLL-2-2A3450), Mayo Clinic-Hem-malignancy program grant (RAF-20P), and State-1 grant (P. Mukherjee); and NIH CA-7838, HL-70567, HL72178-05, and a grant from the American Cancer Society (D. Mukhopadhyay).

The costs of publication of this article were defrayed in part by the payment of page charges. This article must therefore be hereby marked *advertisement* in accordance with 18 U.S.C. Section 1734 solely to indicate this fact.

References

1. Berger AC, Meszoely IM, Ross EA, Watson JC, Hoffman JP. Undetectable preoperative levels of serum CA 19-9 correlate with improved survival for patients with respectable pancreatic adenocarcinoma. Ann Surg Oncol 2004;11:644–9.
2. Shore S, Vimalachandran D, Raraty MG, Ghaneh P. Cancer in the elderly: pancreatic cancer. Surg Oncol 2004;13:201–210.
3. Langer R. Drug delivery and targeting. Nature 1998; 392:5–10.
4. Mendelsohn J. The epidermal growth factor receptor as a target for cancer therapy. Endocr Relat Cancer 2001; 8:3–9.
5. Xiong HQ, Abbruzzese JL. Epidermal growth factor receptor-targeted therapy for pancreatic cancer. Semin Oncol 2002;29:31–7.
6. Hynes NE, Lane HA. ERBB receptors and cancer: the complexity of targeted inhibitors. Nat Rev Cancer 2005; 5:341–54.
7. Rocha-Lima CM, Soares HP, Raez LE, Singal R. EGFR targeting of solid tumors. Cancer Control 2007;14: 295–304.
8. Herbst RS, Kim ES, Harari PM. IMC-C225, an anti-epidermal growth factor receptor monoclonal antibody, for treatment of head and neck cancer. Expert Opin Biol Ther 2001;1:719–32.
9. Kim ES, Khuri FR, Herbst RS. Epidermal growth factor receptor biology (IMC-C225). Curr Opin Oncol 2001;13: 506–13.
10. Kim ES, Lu C, Khuri FR, et al. A phase II study of STEALTH cisplatin (SPI-77) in patients with advanced non-small cell lung cancer. Lung Cancer 2001;34:427–32.
11. Burris H, Storniolo AM. Assessing clinical benefit in the treatment of pancreas cancer: gemcitabine compared to 5-fluorouracil. Eur J Cancer 1997;33 Suppl 1: S18–22.
12. Braakhuis BJ, van Dongen GA, Vermorken JB, Snow GB. Preclinical *in vivo* activity of 2′,2′-difluorodeoxycytidine (Gemcitabine) against human head and neck cancer. Cancer Res 1991;51:211–4.
13. Rosi NL, Giljohann DA, Thaxton CS, Lytton-Jean AK, Han MS, Mirkin CA. Oligonucleotide-modified gold nanoparticles for intracellular gene regulation. Science 2006;312:1027–30.
14. Zharov VP, Kim JW, Curiel DT, Everts M. Self-assembling nanoclusters in living systems: application for integrated photothermal nanodiagnostics and nanotherapy. Nanomedicine 2005;1:326–45.
15. Sokolov K, Follen M, Aaron J, et al. Real-time vital optical imaging of precancer using anti-epidermal growth factor receptor antibodies conjugated to gold nanoparticles. Cancer Res 2003;63:1999–2004.
16. Mukherjee P, Bhattacharya R, Bone N, et al. Potential therapeutic application of gold nanoparticles in B-chronic lymphocytic leukemia (BCLL): enhancing apoptosis. J Nanobiotechnology 2007;5:4.
17. Mukherjee P, Bhattacharya R, Wang P, et al. Antiangiogenic properties of gold nanoparticles. Clin Cancer Res 2005;11:3530–4.
18. El-Sayed IH, Huang X, El-Sayed MA. Surface plasmon resonance scattering and absorption of anti-EGFR antibody conjugated gold nanoparticles in cancer diagnostics: applications in oral cancer. Nano Lett 2005;5:829–34.
19. El-Sayed IH, Huang X, El-Sayed MA. Selective laser photo-thermal therapy of epithelial carcinoma using anti-EGFR antibody conjugated gold nanoparticles. Cancer Lett 2006;239:129–35.
20. Alivisatos P. The use of nanocrystals in biological detection. Nat Biotechnol 2004;22:47–52.
21. Xu X, Han MS, Mirkin CA. A gold-nanoparticle-based real-time colorimetric screening method for endonuclease activity and inhibition. Angew Chem Int Ed Engl 2007;46:3468–70.
22. You CC, Miranda OR, Gider B, et al. Detection and identification of proteins using nanoparticle-fluorescent polymer "chemical nose" sensors. Nat Nanotech 2007;2: 318–23.
23. Whitesides GM. The "right" size in nanobiotechnology. Nat Biotechnol 2003;21:1161–5.
24. Whitesides GM, Kriebel JK, Love JC. Molecular engineering of surfaces using self-assembled monolayers. Sci Prog 2005;88:17–48.
25. Higby GJ. Gold in medicine: a review of its use in the West before 1900. Gold Bull 1982;15:130–40.
26. Daniel MC, Astruc D. Gold nanoparticles: assembly, supramolecular chemistry, quantum-size-related properties, and applications toward biology, catalysis, and nanotechnology. Chem Rev 2004;104:293–46.
27. Boal AK, Ilhan F, DeRouchey JE, Thurn-Albrecht T, Russell TP, Rotello VM. Self-assembly of nanoparticles into structured spherical and network aggregates. Nature 2000;404:746–8.
28. Hainfeld JF, Slatkin DN, Focella TM, Smilowitz HM. Gold nanoparticles: a new X-ray contrast agent. Br J Radiol 2006;79:248–53.
29. Goodman CM, McCusker CD, Yilmaz T, Rotello VM. Toxicity of gold nanoparticles functionalized with cationic and anionic side chains. Bioconjug Chem 2004;15:897–900.
30. Zahr AS, de Villiers M, Pishko MV. Encapsulation of drug nanoparticles in self-assembled macromolecular nanoshells. Langmuir 2000;21:403–10.
31. Bhattacharya R, Patra CR, Verma R, Kumar S, Greipp PR, Mukherjee P. Gold nanoparticles inhibit proliferation of multiple myeloma cells. Adv Mater 2007;19:711–6.
32. Bhattacharya R, Mukherjee P, Xiong Z, Atala A, Soker S, Mukhopadhyay D. Gold nanoparticles inhibit VEGF165-induced proliferation of HUVEC cells. Nano Lett 2004;4:2479–81.
33. Bhattacharya R, Patra CR, Earl A, et al. Attaching folic acid on gold nanoparticles using noncovalent interaction via different polyethylene glycol backbones and targeting of cancer cells. Nanomed 2007;3:224–38.
34. Stephan S, Datta K, Wang E, et al. Effect of rapamycin alone and in combination with antiangiogenesis therapy in an orthotopic model of human pancreatic cancer. Clin Cancer Res 2004;10:6993–7000.
35. Freeman KB, Anliker S, Hamilton M, et al. Validated assays for the determination of gemcitabine in human plasma and urine using high-performance liquid chromatography with ultraviolet detection. J Chromatogr B Biomed Appl 1995;665:171–81.
36. Mangeney C, Ferrage F, Aujard I, et al. Synthesis and properties of water-soluble gold colloids covalently derivatized with neutral polymer monolayers. J Am Chem Soc 2002;124:5811–21.
37. Bhattacharya R, Patra CR, Wang S, et al. Assembly of gold nanoparticles in a rod-like fashion using proteins as templates. Adv Funct Mater 2006;16:395–400.
38. Bourg MC, Badia A, Lennox RB. Gold-sulfur bonding in 2D and 3D self-assembled monolayers: XPS characterization. J Phys Chem B 2000;104:6562–7.
39. Kumar A, Mukherjee P, Guha A, et al. Amphoterization of colloidal gold particles by capping with valine molecules and their phase transfer from water to toluene by electrostatic coordination with fatty amine molecules. Langmuir 2000;16:9775–83.
40. Demers LM, Ostblom M, Zhang H, Jang NH, Liedberg B, Mirkin CA. Thermal desorption behavior and binding properties of DNA bases and nucleosides on gold. J Am Chem Soc 2002;124:11248–9.
41. Bruns CJ, Shrader M, Harbison MT, et al. Effect of the vascular endothelial growth factor receptor-2 antibody DC101 plus gemcitabine on growth, metastasis and angiogenesis of human pancreatic cancer growing orthotopically in nude mice. Int J Cancer 2002;102: 101–8.